The Coplanar Resonator Technique for Determining the Surface Impedance of $YBa_2Cu_3O_{7-\delta}$ Thin Films

A. Porch, M. J. Lancaster, *Member, IEEE,* and R. G. Humphreys

Abstract— We describe how coplanar microwave resonators fabricated from patterned thin films of $YBa_2Cu_3O_{7-\delta}$ (YBCO) can be used to measure the ab-plane microwave surface impedance $Z_s = R_s + jX_s$ of the films, in particular the absolute value and temperature dependence of the magnetic penetration depth λ. The current distribution of the resonator is calculated by modelling the resonator as a network of coupled transmission lines of rectangular cross-sections; this is then used to estimate the ab-plane $\lambda(T)$ from the measurements of resonators of different geometries patterned onto the same film. We obtain values of $\lambda(0)$ in the range 150–220 nm. The unloaded quality factors of the linear resonators at 7.95 GHz are around 45000 at 15 K and around 6500 at 77 K. We estimate the corresponding values of the intrinsic R_s at 7.95 GHz to be 23 $\mu\Omega$ and 110 $\mu\Omega$ at 15 K and 77 K, respectively. These values are comparable with those of other high quality unpatterned YBCO films reported in the literature. Z_s for the best optimised films appears to be insensitive to the effects of patterning.

I. INTRODUCTION

THE BASIS OF most microwave devices is the planar transmission line and the characterization of lines fabricated from high-T_c materials is crucial to the development of these materials for microwave applications. Microwave coplanar transmission lines are some of the simplest examples of planar transmission lines and are often used as planar chip interconnects, which can be used as resonant elements in oscillator circuits. The benefits of using superconducting films over conventional metal films such as gold in these applications are to provide low-loss lines and very high-Q resonators.

For microwave applications, it is important to characterize patterned films and assess the effects of film patterning. The coplanar transmission line resonator is an ideal structure for characterizing patterned films of high-T_c materials since only one film surface is required, thus removing the need for double-sided depositions. Additionally, the high edge current densities in the coplanar geometry emphasizes any effects due to the patterning.

There have been many reports in the literature of experiments involving coplanar YBCO thin film structures. These include microwave surface impedance determination [1]–[8], microwave absorption studies [9], very high frequency pulse propagation studies [10]–[12], and potential applications such as delay lines [13] and filters [14]. The aim of this paper is to present our own microwave measurements of YBCO films using the coplanar resonator technique and to show how it can be used to estimate *absolute* values of the microwave surface impedance Z_s.

The microwave current density in a coplanar resonator is very sharply peaked at the edges of the central strip and the ground planes adjacent to the central strip, particularly when the magnetic penetration depth λ is smaller than the film thickness t. For c-axis oriented films, the microwave currents are constrained to flow along the ab-planes. Provided we first calculate the current distribution on the resonator cross-section, we can calculate the ab-plane surface impedance $Z_s = R_s + jX_s = R_s + j\omega\mu_0\lambda$ from the measurements of resonant bandwidths and frequency shifts for temperatures below T_c. We will now discuss our experimental method and subsequent numerical analysis in detail.

II. EXPERIMENTAL DETAILS

The YBCO films are grown by co-evaporation in an atomic oxygen atmosphere in an ultra-high-vacuum evaporator using electron-beam-heated sources for each of the Y, Ba, and Cu metals. The cation composition is controlled by a quadrupole mass spectrometer and gives high compositional accuracy [15]. The substrates are polished (001)-oriented MgO single crystals, which are ion milled *in situ* prior to growth. A homoepitaxial buffer layer of 10–20 nm of MgO is then grown by Mg evaporation prior to the growth of the YBCO. The deposition temperature is typically 690°C, at a rate of 0.1 nms^{-1}, with standard resulting film thicknesses of 350 nm. Misalignment of the films' c-axis orientation relative to the substrate normal depends on the substrate misorientation, and is measured to be less than 1%. The films are silvered for contact purposes at the ground plane edges by silver evaporation and are then patterned by photolithography into the linear and meander structures illustrated in Fig. 1 by a combination of argon ion beam milling and subsequent ethylene diamine tetra-acetic acid (EDTA) wet etching through a photoresist mask. The purpose of the wet etch is to remove
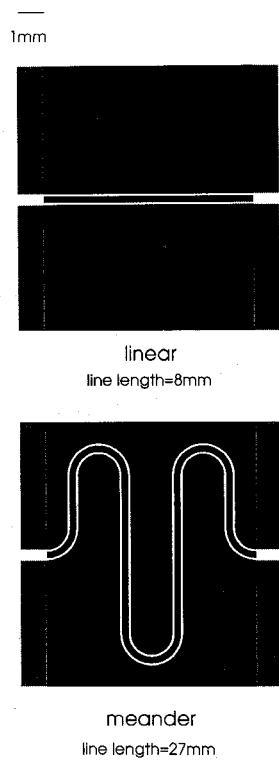
linear
line length=8mm

meander
line length=27mm

Fig. 1.   The geometry of the linear and meander coplanar resonators.The standard 50-Ω lines have a central line width of $W = 200$ μm,with a gap to each ground plane $S = 73$ μm. The films are 10 mm$\times$ 10 mm square. The shaded areas at the end of each groundplane represent the silver contact pads.

Fig. 2.   Schematic diagram of the microwave package.

any possibly ion-damaged material at the film edges. In practice, the YBCO-free regions tend to be around 2 μm wider than the mask dimensions due to the wet etch. The films are then annealed at 500°C in 1bar of O_2 for 30 minutes to improve the film oxygenation and contact adhesion to the substrate. This annealing also improves the contact adhesion of the silver to the YBCO film.

The T_c of the resulting films varies between 88–91 K, with highest dc J_c measured to be around 2×10^6 Acm^{-2} at 77 K, and in excess of 10^7 Acm^{-2} below 20 K. Our resonator geometry is chosen so that our standard resonator has a characteristic impedance of 50 Ω, with a strip width $W = 200\mu$m and a spacing to each ground plane $S = 73$ μm. We also have another geometry with S around 12 μm to enable us to study kinetic inductance effects more precisely. The line length of the linear resonator is 8 mm, while the total line length of the meander resonator is 27 mm, with three semi-circular and two quarter circle bends.

We package our resonators in the flip-chip brass assembly illustrated in Fig. 2. Microwave power is coupled capacitively into the resonator using Wiltron K-connectors. Contacts between the silvered portions of the ground planes and the ledge on the wall of the housing are provided by four thin layers of indium foil. The resonator is spring-loaded onto these edges to maintain good ground plane contacts as the temperature changes. It is essential to keep both ground planes electrically balanced during this experiment, otherwise unwanted slotline resonances can appear.
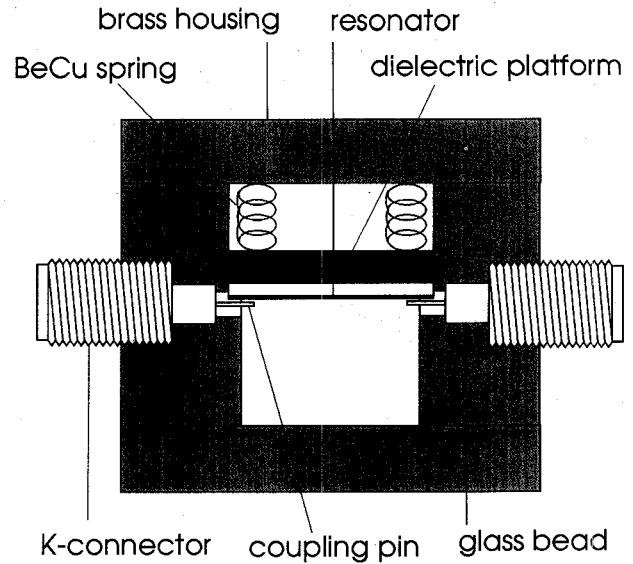
The package is mounted inside a closed-cycle cooler and the transmitted microwave power is measured as a function of frequency and temperature in the ranges 2–20 GHz and 12 K-T_c using a Hewlett Packard 8720 A network analyzer. The spectral responses of a linear and meander resonator at 77 K are shown in Fig. 3. At low temperatures, the meander resonator has a fundamental resonance around 2.36 GHz, while the linear resonator has a fundamental around 7.95 GHz.

We measure the full resonant bandwidth at half power f_B and resonant frequency f as a function of temperature, from which we determine the loaded quality factor $Q_L = f/f_B$. The unloaded quality factor Q_0 is calculated from Q_L and the insertion loss I at resonance using the relation $Q_0 = Q_L/(1 - |S_{12}|)$, where $|S_{12}| = 10^{-I/20}$. We usually fix I to be in the region between 20 and 30 dB, such that Q_0 differs little from Q_L. We are unable to account adequately for the change in the loss of the input and output cables as a function of temperature, but at these high values of I this results in a systematic overestimate of Q_0 of only around 1%. The highest values of Q_0 range from 45000 at 12 K to 6500 at 77 K for the fundamental mode of a linear resonator at 7.95 GHz. These values of Q_0 for the linear resonator are more than two orders of magnitude higher than our measurements of similar copper linear coplanar resonators for temperatures below 80 K.

In Fig. 4(a), we plot Q_0 as a function of temperature for the first two modes of our best linear resonator, and in Fig. 4(b) we plot the corresponding resonant frequency shift as a function of temperature for the fundamental. No measurements are possible in the normal state where the resonators are highly dissipative. The microwave response is approximately independent of microwave power for input powers up to +10 dBm at low T (corresponding to edge current densities in excess of 10^6 Am^{-2}). All the measurements presented here are for low input powers where nonlinear effects are absent, allowing us to determine unambiguous values of Q_0 from the half-power bandwidths and insertion losses.
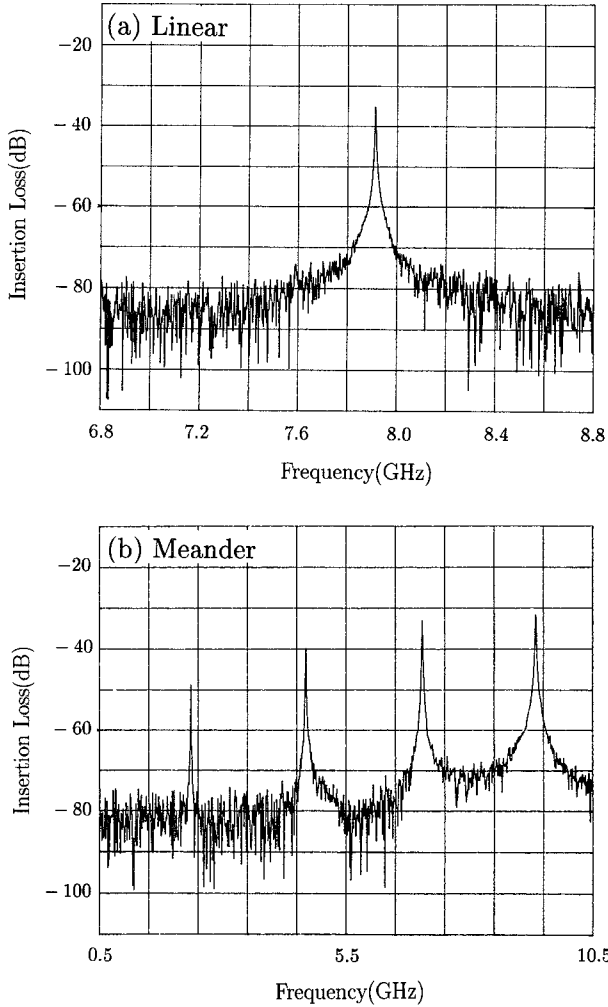
Fig. 3. The transmitted microwave power as a function of frequency at 77 K for (a) a linear resonator and (b) a meander resonator.
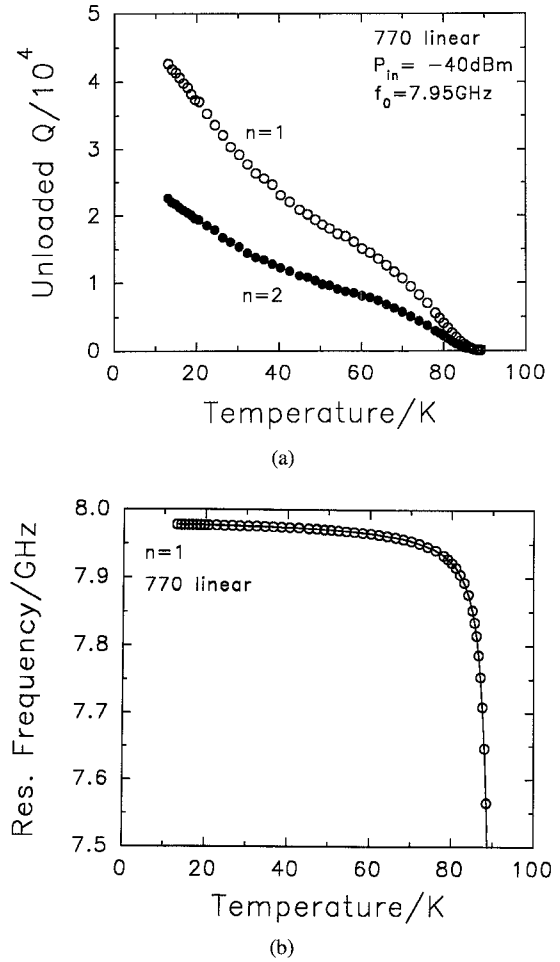

Fig. 4. (a) The unloaded quality factor Q_0 as a function of temperature for the first two modes of a linear resonator. The difference in Q_0 between the two modes is a consequence of the frequency dependent surface resistance of the YBCO film. (b) The resonant frequency as a function of temperature for the fundamental of a linear resonator. The rapid decrease in frequency as T approaches T_c from below is due to the rapid increase in $\lambda(T)$.

III. MICROWAVE THEORY

The surface resistance R_s and surface reactance X_s of the films can be obtained from the measurements of Q_0 and resonant frequency f, respectively, of the resonators. The losses of any resonator are additive, so we can write

$$\frac{1}{Q_0} = \frac{1}{Q_c} + \frac{1}{Q_d} + \frac{1}{Q_{\mathrm{rad}}} \tag{1}$$

where Q_c, Q_d and Q_{rad} are the conductor, dielectric and radiation quality factors, respectively. We find that both Q_d and Q_{rad} are very large (we will return to this later in Section IV-B). The measured unloaded quality factor is then determined predominantly by the dissipation in the conductors. Likewise, the total resonant frequency shift is the sum of the shift Δf due to changes in $\lambda(T)$ and other terms mainly due to the changes in the resonator length and substrate dielectric constant. Before we can relate the changes in resonator response to Z_s of the films, we have to calculate the current distribution in the resonator, since this distribution is highly dependent on the ratio λ/t (where t is the film thickness).

A. Coupled Transmission Line Calculation

We calculate the volume current distribution as a function of λ using the method of Weeks et al. [16], recently modified to superconducting planar transmission lines by Sheen et al. [17]. This method has been discussed in detail by these other authors, but we will describe it again here in the context of the coplanar geometry.

We consider the cross-section of a coplanar transmission line to consist of a network of parallel superconducting transmission lines of varying rectangular cross-sectional areas ("patches"). We chose these patches to be smallest where the current density changes most rapidly (i.e., at the film corners), as shown schematically in Fig. 5. Consider the line cross-section lying in the xy-plane and suppose we have a total number of patches N along the y-axis of the center conductor, which has total width W. To determine the y-axis coordinates of the corners of the patches on the center conductor, we use the following procedure: We choose the width along the y-axis of the smallest patch to be some small fraction α of λ (typically, we choose $\alpha = 1/10$). Next, we
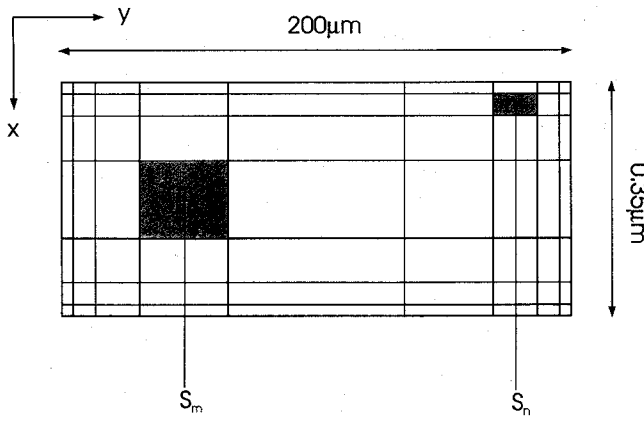
Fig. 5. A schematic diagram illustrating the patch distribution over the cross-section of the center conductor used in the calculation of the current distribution.

assume that the neighbouring patch has a y-axis width some factor β (> 1) larger than the smallest patch, and we scale each adjacent patch by the same scaling factor β, leaving the largest patch in the middle of the center line. The quantity β is then found by taking the positive real root (>1) of the polynomial

$$\alpha\lambda\left(1 + \beta + \beta^2 + \beta^3 + \cdots + \beta^{(N-3)/2} + \frac{1}{2}\beta^{(N-1)/2}\right) - \frac{W}{2} = 0 \quad (2)$$

If $N\lambda > W$ we ensure that each of the patches has the same width. We use exactly the same procedure to establish the x-axis coordinates of the patch corners (the scaling factor β will, of course, be different); the smallest patch is then a square of area $(\alpha\lambda)^2$ positioned at the corners of the center conductor.

To determine the y-axis coordinates of the patch corners on the ground planes, we use a slightly different approach. Again we assume that the smallest patch has a y-axis width $\alpha\lambda$. If we assume that the width of the ground plane is W_g, with a total number of patches N_g along the y-axis, then we find the scaling factor β' for ground plane patches by taking the positive real root (> 1) of the polynomial

$$\alpha\lambda(1 + \beta' + \beta'^2 + \beta'^3 + \cdots + \beta'^{(N_g-1)/2}) - W_g = 0 \quad (3)$$

Since the structure is coplanar, the x-axis coordinates of the patch corners on the ground planes will be the same as those on the center conductor. The smallest ground plane patches again have area $(\alpha\lambda)^2$, positioned at the corners of the ground plane adjacent to the center conductor. The largest ground plane patches are positioned at the edges of the cross-section furthest away from the center conductor.

Having set up the distribution of patches for the one value of λ, we proceed to calculate the line inductance per unit length $L(\lambda)$. We first consider the external (geometrical) inductance per unit length l^{ext} of the network. If the dimension of the patches is small enough where the current density changes most rapidly, then the current distribution across each patch is approximately uniform. In this case, from stored energy

concepts it can be shown that the external inductance between two lines of areas S_m and S_n is [16]

$$l_{mn}^{\text{ext}} = -\frac{\mu_0}{4\pi S_m S_n}$$
$$\times \int_{S_m}\int_{S_n} \ln[(x - x')^2 + (y - y')^2]\,dxdydx'dy' \quad (4)$$

where we consider the patches to be in the xy-plane with microwave currents along the z-axis. This integral can be solved analytically [16], [17] for a network of rectangular patches using integration by parts. The diagonal terms in l^{ext} are the self inductances of each of the lines, while off-diagonal terms are the mutual inductances between pairs of lines.

To include the effects of the superconductor on the total line inductance we introduce an internal inductance in series with l^{ext}, represented by the matrix l^{int}, which we define below. For a superconductor, l^{int} is a sum of two terms: the magnetic inductance, due to the magnetic energy stored within the film volume owing to the finite λ, and the kinetic inductance, due to the nondissipative kinetic energy of the supercurrent. In thin films with $\lambda \sim t$, the largest contribution to l^{int} is due to the kinetic inductance.

Much of the experimental data of others imply that YBCO is in the local London limit, where the electronic mean free path ℓ is larger than the superconducting coherence length ξ_0. In this limit $Z_s = (j\omega\mu_0/\sigma)^{1/2}$, where the superconductor conductivity is written conventionally as $\sigma = \sigma_1 - j\sigma_2$. We need to distinguish between the measured penetration depth and the static penetration depth in the London limit λ_L (where $\lambda_L = (\omega\mu_0\sigma_2)^{-1/2}$). Here we introduce a complex penetration depth λ, defined by $Z_s = (j\omega\mu_0/\sigma)^{1/2} = j\omega\mu_0\lambda$, where

$$\frac{1}{\lambda^2} = \frac{1}{\lambda_L^2} + j\omega\mu_0\sigma_1 \quad (5)$$

Our measured penetration depth is then the real part of λ. However, provided we are not too close to T_c (i.e. $\sigma_1 \ll \sigma_2$) λ is approximately real and equal to λ_L (we will always restrict ourselves to this limit and from here on we will drop the subscript L in λ_L); consequently $\sigma \simeq \sigma_1 - j/\omega\mu_0\lambda^2$.

We pick an arbitrary patch (labelled patch 0) to act as a reference from which all voltages are measured. The variation of voltage of the nth patch relative to the reference patch ΔV_n as a function of distance z along the line is then given by [16], [17]

$$-\frac{\partial}{\partial z}\Delta V_n = \sum_{m>0}(r_{mn} + j\omega l_{mn})i_m \quad (6)$$

where i_m is the current on the mth patch. The line resistance matrix r defined by (6) is

$$r_{mn} = \text{Re}\left(\frac{1}{\sigma S_0} + \frac{1}{\sigma S_n}\delta_{mn}\right) \quad (7)$$

where $\delta_{mn} = 1$ if $m = n$ and 0 otherwise. The inductance matrix l of (6) is then

$$l_{mn} = l_{mn}^{\text{int}} + l_{mn}^{\text{ext}} - l_{m0}^{\text{ext}} - l_{0n}^{\text{ext}} + l_{00}^{\text{ext}} \quad (8)$$
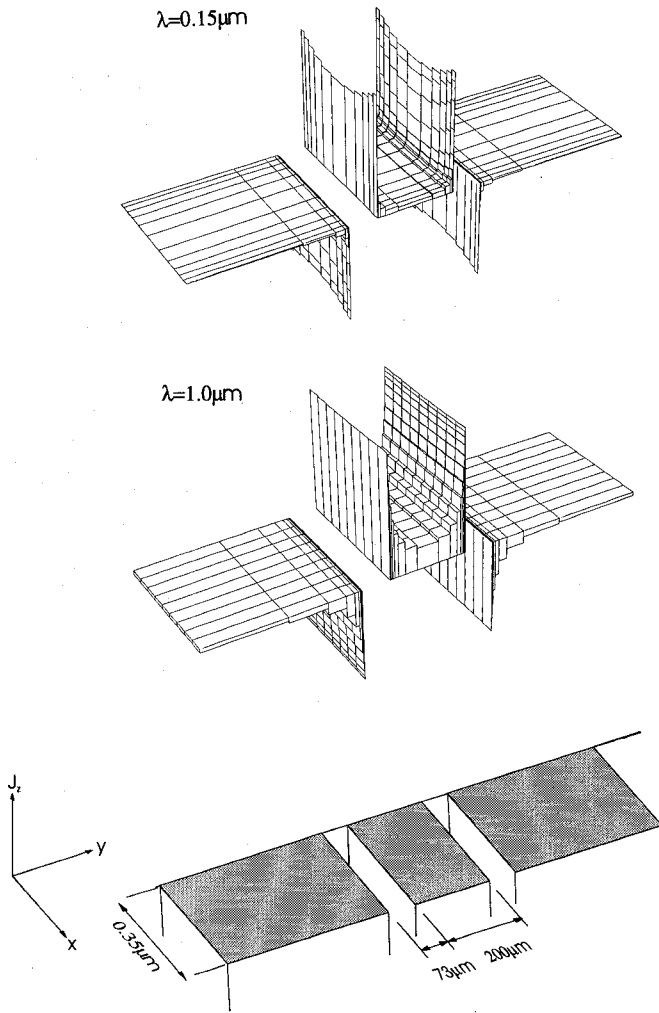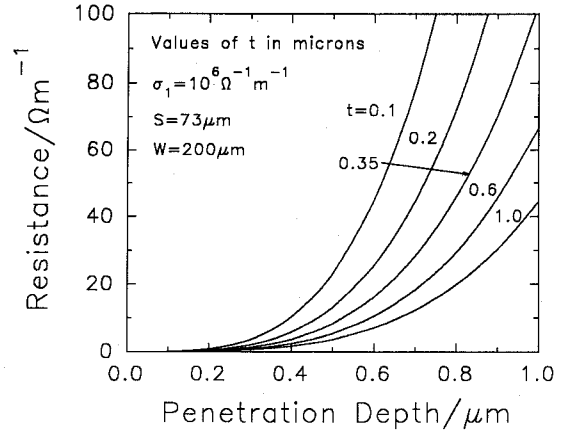
Fig. 6. The current distribution on the resonator cross-section calculated for $\lambda = 0.15 \ \mu$m and 1.0 μm. As λ increases the current distribution becomes more uniform.

Fig. 7. (a) The theoretical variation of line resistance per unit length $R(\lambda)$ for various film thicknesses; (b) the theoretical variation of the line inductance per unit length $L(\lambda)$ for various film thicknesses. These plots allow us to calculate $g_1(\lambda)$ and $g_2(\lambda)$ as a function of t for fixed values of S and W.

By analogy with the formulation of the resistance matrix, the internal inductance matrix l^{int} is defined as
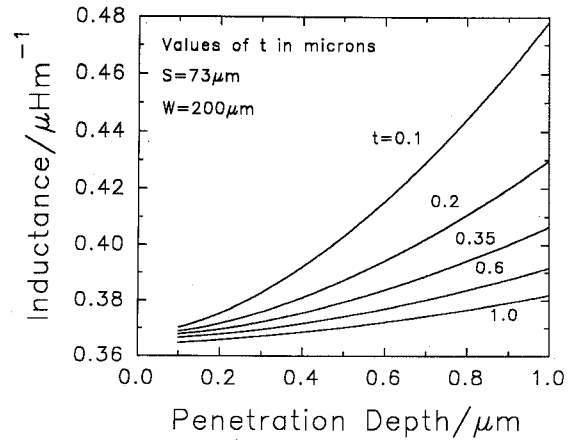
$$l^{\text{int}}_{mn} = \frac{1}{\omega}\text{Im}\left(\frac{1}{\sigma S_0} + \frac{1}{\sigma S_n}\delta_{mn}\right) \qquad (9)$$

For simplicity, we assume that the line voltages ΔV_n are quasistatic, with each pair of lines experiencing the same *effective* dielectric constant $\varepsilon_{\text{eff}} \simeq (\varepsilon_r + 1)/2$. We find experimentally that the harmonics of our resonators have resonant frequencies approximately at integer multiples of the fundamental frequency. Consequently, we expect this quasistatic TEM modelling to be a good approximation to the real case. If we take the reference patch somewhere on the center conductor, then $\Delta V_n = 0$ for all patches on the center conductor; we then arbitrarily take $\Delta V_n = 1$ for patches on either of the ground planes. To calculate the currents i_n for one particular value of λ, we need to invert the impedance matrix per unit length $Z = r + j\omega l$ assuming the quasistatic form for ΔV, i.e.

$$i = -Z^{-1}\frac{\partial}{\partial z}\Delta V = j\gamma(r + j\omega l)^{-1}\Delta V \qquad (10)$$

where γ is the complex propagation constant of the network. The calculated current distribution is shown in Fig. 6.

If we define I_{tot} as the magnitude of the total current carried on the center conductor (which is the same magnitude as the total current carried on the two ground planes), then the resonator resistance per unit length R can be calculated from

$$I^2_{\text{tot}}R = \sum_n i^2_n R'_n \qquad (11)$$

where $R'_n = \text{Re}(1/\sigma S_n)$ and S_n is the area of the nth patch. Similarly, for the inductance per unit length L

$$I^2_{\text{tot}}L = \sum_{mn} i_m L'_{mn} i_n \qquad (12)$$

where $L'_{mn} = l^{\text{ext}}_{mn} + l^{\text{int}}_{mn}$. The currents i_m and i_n in (11) and (12) are the current magnitudes on the mth and nth patches, respectively. We normally work with a total number of patches of 315. This is low enough to ensure that computing time is not too long, but large enough not to limit the accuracy of the computed values of R and L. The results for $R(\lambda)$ and $L(\lambda)$ are shown in Fig. 7 for various values of film thickness for the standard (50 Ω) line geometry.

To enable us to perform quick calculations using these results, we confine ourselves to the limit where $\sigma_1 \ll \sigma_2$ (i.e. $\sigma_1 \omega \mu_0 \lambda^2 \ll 1$), which we would expect to be valid for YBCO to within 2 K of T_c and for frequencies below 100 GHz. In this limit, we find that

$$L(\lambda) \simeq \mu_0 g_1(\lambda) = \frac{X_s}{\omega \lambda} g_1(\lambda) \qquad (13)$$

and

$$R(\lambda) \simeq \frac{1}{2} \mu_0^2 \sigma_1 \omega^2 \lambda^3 g_2(\lambda) = R_s g_2(\lambda) \qquad (14)$$

where g_1 and g_2 are also functions of resonator geometry. If we can find the absolute value and temperature dependence of λ then we can calculate g_1 and g_2 as a function of temperature for any geometry. We now show how $Z_s = R_s + jX_s$ can be calculated using g_1 and g_2 from the data for the resonant bandwidths f_B and frequency shifts Δf.

IV. ANALYSIS OF THE RESULTS

A. Calculation of $\lambda(T)$

It is clear from the numerical results of Section III that it is critical that we first determine the *absolute* value of $\lambda(T)$ before we can calculate the film surface impedance. This is difficult to achieve in practice. It is commonplace to assume a value $\lambda(0)$ and then vary this parameter until $\lambda(T)$ fits the forms given by the BCS theory in the London limit or the Gorter-Casimir model. There is growing evidence that suggests that $\lambda(T)$ in YBCO is quite unlike that observed in any of the conventional superconductors, particularly at low temperatures, so that fitting $\lambda(T)$ to any conventional theory as a means of calculating $\lambda(0)$ is inadequate.

In principle, we could calculate the absolute value of λ at any temperature by the measurement of the absolute resonant frequency alone, but this would require the measurement of the resonator dimensions to a scale less than λ itself, which is difficult on practical grounds. Hence, we are confined to measuring the changes in resonant frequency $\Delta f(T) = f(T_0) - f(T)$, where T_0 is a fixed low temperature that we usually take to be around 12 K (i.e., the lowest attainable temperature of our measuring system). Note that we define this frequency shift to be a positive quantity (here the resonant frequency always decreases as the temperature is increased). We approximate the fractional frequency shift $\Delta f(T)/f(T)$ as a sum of three main terms

$$\frac{\Delta f(T)}{f(T)} \simeq \frac{1}{2} \frac{\Delta \varepsilon_r}{\varepsilon_r} + \frac{\Delta l}{l} + \frac{1}{2g_1} \frac{\partial g_1}{\partial \lambda} \Delta \lambda \qquad (15)$$

where we associate the first two terms as being due to the changes in dielectric constant ε_r and length l of the substrate, respectively, as a function of temperature; the third term is the inductance term, i.e. the frequency shift due to changes in λ as a function of temperature. The substrate terms in (15) are approximately independent of frequency, so they cannot be evaluated by measuring the frequency shifts of a number of different modes. The inductance term is also independent of frequency in the limit $\sigma_1 \ll \sigma_2$. In Fig. 8 we plot $\Delta f/f$ as a
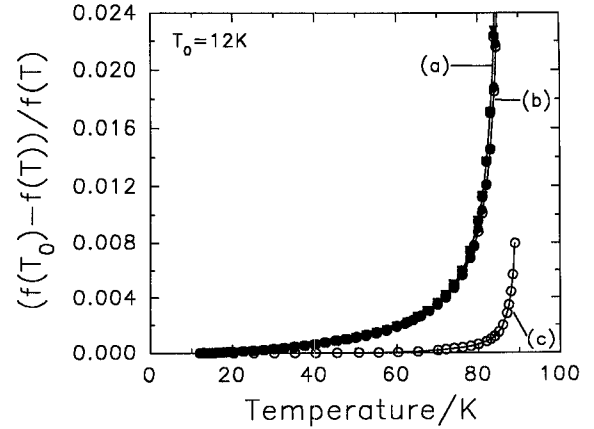

Fig. 8. The fractional frequency shift $\Delta f/f$ as a function of temperature for (a) the first two modes of a linear resonator, and (b) the first four modes of a meander resonator; (c) is $\Delta f/f$ as a function of temperature for a microstrip resonator constructed from one of the ground planes of the linear resonator.

function of temperature for the first four modes of a meander resonator and the first two modes of a linear resonator. Apart from a slight difference in T_c between the two resonators, all of the plots lie on the same curve, indicating that λ is frequency independent well below T_c (thus implying a supercurrent response $\sigma_2 \propto 1/\omega$, as expected in the London limit); the differences between curves (a) and (b) in Fig. 8 can be attributed to a 1 K difference in T_c.

The inductance term of (15) should be much larger than the substrate terms, particularly close to T_c, but we need to quantify these latter terms at lower temperatures before we attempt to extract $\lambda(T)$ from this data. Hence, we cleaved off one of the ground planes of the linear resonator of Fig. 8 and constructed a microstrip resonator above a copper ground plane using the MgO substrate as the dielectric spacer. Although the geometry factor g_1 is different for this microstrip resonator, the substrate terms should be nearly the same (we find experimentally that the frequency shift due to kinetic inductance effects is much smaller for this resonator than for the coplanar resonator since the dielectric spacer thickness is 0.7 mm). The data for $\Delta f/f$ as a function of temperature for the microstrip resonator is shown in curve (c) of Fig. 8. We find that the substrate terms contribute less than 10^{-5} to the overall $\Delta f/f$ below 60 K, and any contribution between 60 K and T_c is much smaller than the kinetic inductance term. This information allows us to make the approximation that all of the measured frequency shifts with temperature are due to the changes in $\lambda(T)$. This is particularly important at low T, where we note that $\Delta f/f$ changes more rapidly than would be expected if $\lambda(T)$ was described by the BCS theory in the London limit.

However, we still have no way of finding $\lambda(T)$ absolutely, since at each temperature the data for $\Delta f/f$ for a single resonator contains two unknowns, namely $\lambda(T)$ and $\lambda(T_0)$. To solve this problem, we patterned two identical resonators of the same geometry parallel and adjacent to each other on the same YBCO film and separated the pair by cleaving. When measured, these resonators gave the same $\Delta f/f$ to within 0.5% from low T to within 2 K of T_c, indicating the
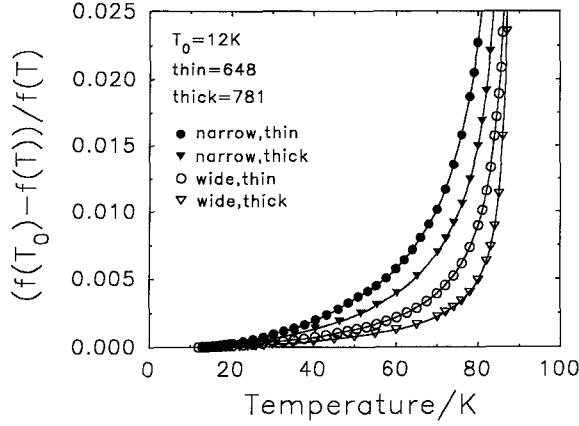
Fig. 9. The fractional frequency shift $\Delta f / f$ as a function of temperature for the fundamentals of four linear resonators of different cross-sectional geometries. Here, the wide and narrow gap resonators correspond to $S = 73$ μm and 12 μm, respectively; the thick and thin films correspond to $t = 0.7$ and 0.35 μm, respectively.

Fig. 11. The surface resistance R_s as a function of temperature calculated from the data for $\lambda(T)$ for the first two modes of a linear resonator with a fundamental resonant frequency of 7.95 GHz. This plot illustrates the quadratic frequency dependence of R_s.
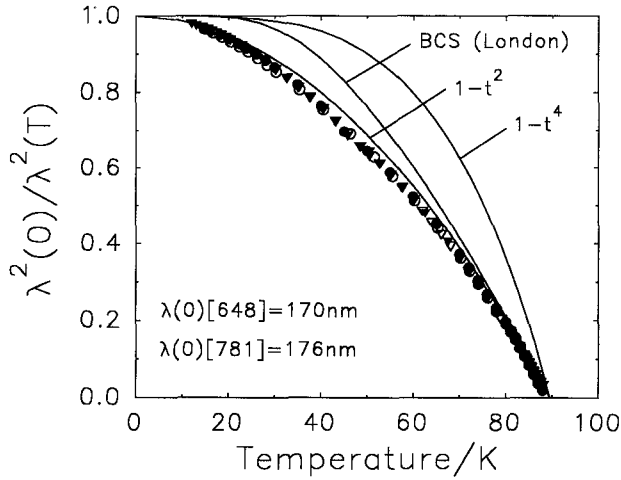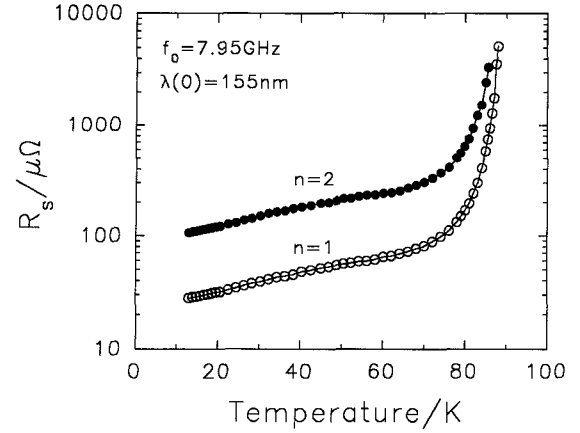

Fig. 10. The data of Fig. 9 processed to give the temperature dependence of $\sigma_2 \propto 1/\lambda^2$. The form of σ_2 is the same for all of the resonators, with slightly different values of $\lambda(0)$. Also shown is the result of the BCS theory in the clean limit ($\ell > \xi_0$) of the local theory ($\ell < \lambda$), i.e. the BCS London limit, and the empirical functions $1 - t^4$ (which serves as an approximation to the BCS theory including the effects of strong coupling) and $1 - t^2$ (where t is the reduced temperature T/T_c).

high uniformity of film thickness and film properties across the film surface. We also patterned two adjacent resonators of different geometries onto the same film, one with the standard ("wide") gap of $S = 73$ μm, the other with a smaller ("narrow") gap of $S = 12$ μm. The gap widths could be measured to ± 0.5 μm accuracy using a high-power optical microscope. For each resonator, we now have two different geometry factors g_1^{narrow} and g_1^{wide}, giving different values for $\Delta f / f$ at each temperature. In Fig. 9, we plot $\Delta f / f$ for two parallel resonators of the wide and narrow gap geometries for our standard film thickness of 0.35 μm and also for wide and narrow resonators of thickness 0.7 μm. For each pair of resonators and at any fixed temperature T we now have two values of $\Delta f / f$ and two unknowns, namely $\lambda(T)$ and $\lambda(T_0)$. Our analysis now proceeds along the following lines. For each temperature T we assume a

value of $\lambda(T_0)$ (which for simplicity we call λ_0 in the following discussion). We can calculate the theoretical value of $\Delta f(\lambda, \lambda_0)/f(\lambda, \lambda_0) = \Delta L(\lambda, \lambda_0)/2L(\lambda, \lambda_0)$, and then by comparison with the experimental data of $\Delta f(T)/f(T)$ we calculate $\lambda(T)$ using the assumed value of λ_0. We perform this analysis for the data for each geometry. Since the values of $\lambda(T)$ and λ_0 are the same for each resonator for the same values of T and T_0, we adjust λ_0 so that the two plots for $\lambda(T)$ for each resonators agree.

The results of the analysis for the data of Fig. 9 is shown in Fig. 10. Extrapolating $\lambda(T)$ to $T = 0$, we obtain values of $\lambda(0)$ in the range between 150 and 220 nm for our resonators. We find that the values of $\lambda(0)$ depend critically on the measured values of S for the narrow gap resonators. All random errors are small, but a systematic error of ± 1 μm in S around the average value of 12 μm results in a ± 30 nm error in $\lambda(0)$. We can measure widths to an accuracy of better than ± 0.5 μm, but our line edges are uniform only to within ± 0.5 μm, with further systematic error due to the precise shape of the edge cross section (our analysis assumes that the corners are square). Errors in t are around $\pm 2\%$, and are found to be negligible in comparison. Our absolute values of $\lambda(0)$ are therefore in error by around $\pm 10\%$, although the temperature dependence of λ is relatively unaffected by this error. In fact, this method allows us to measure very small changes in λ very accurately. For example, at low T, the experimental error in determining the fractional resonant frequency shift $\Delta f / f$ is less than $\pm 10^{-6}$, giving an upper limit of the error in $\Delta \lambda$ of around $\pm 10^{-4} \lambda(0)$.

B. Calculation of $R_s(T)$

Having determined $\lambda(T)$ for a pair of resonators, it is a straightforward matter to obtain the surface resistance $R_s(T)$ for either resonator. Provided we restrict the analysis to temperatures not too close to T_c, it can be seen from (14) that the line resistance $R(\sigma_1, \lambda)$ is approximately proportional to σ_1. At each temperature, we first compute the theoretical conductor bandwidth $f_{B,c} = R(\sigma_1, \lambda)/2\pi L(\lambda)$ for a trial value of σ_1 (e.g. $\sigma_1 = 10^6$ $\Omega^{-1}\text{m}^{-1}$) using the previously determined $\lambda(T)$. By comparing this theoretical bandwidth

with the experimental bandwidth we then determine $\sigma_1(T)$; from $\sigma_1(T)$ we calculate $R_s = \mu_0^2 \omega^2 \sigma_1 \lambda^3/2$. The results for $R_s(T)$ for the first two modes of a linear resonator are shown in Fig. 11. Our best values of R_s at 8 GHz range from 23 $\mu\Omega$ at 15 K, rising to 110 $\mu\Omega$ at 77 K. These values compare favourably with the best values of R_s for patterned films reported in the literature [18] and are only a factor of around 2 greater than those for the best unpatterned films [19]. There is a systematic error of around $\pm 30\%$ in our values of R_s owing to the systematic error in the absolute value of λ (this systematic error is much greater than the $< \pm 1\%$ error in determining the experimental bandwidths).

We have associated all of the measured dissipation with conductor loss. There will be other losses due to radiation and losses in the dielectric. We are unable to measure the radiation loss, but theoretically we expect that $Q_{\mathrm{rad}} > 10^6$ for temperatures below 80 K. Consequently, we assume that our results are unaffected by radiation loss. If we assume that R_s is proportional to ω^2 then the conductor quality factor Q_c is proportional to $1/\omega$. We find that our measured quality factors Q_0 are approximately proportional to $1/\omega$, and we associate any slight discrepancy as being due to the finite loss tangent of MgO. At low T this sets a lower limit on Q_d of 5×10^5, so that our results are only slightly affected by the finite loss tangent of the substrate (at low T, ignoring the effects of dielectric loss leads to an overestimate of R_s at 16 GHz of less than 5%). At 77 K we find $Q_0 \propto 1/\omega$ to within our experimental error, so that the effects of substrate loss are negligible compared to conductor loss at this temperature.

V. CONCLUSIONS AND SUMMARY

We have obtained results for Z_s on a range of thin film YBCO samples using the coplanar resonator method. We have not yet optimized our film patterning process or any subsequent reannealing stages. For our earliest films, we believed that patterning damage may have been the limiting factor that degraded Z_s in our films due to edge damage. However, the low values of R_s and the improved microwave field handling capabilities of our recent films patterned in the same way implies that growth conditions, and not necessarily the patterning itself, limits the performance of the films [2].

The coplanar technique allows an accurate measurement of changes in $\lambda(T)$, in addition to an estimate of the absolute value of $\lambda(0)$. Our results for the temperature dependence of λ in YBCO films are of interest, particularly at low T. When plotting σ_2 as a function of temperature at low T, we find that the ratio $\sigma_2(T)/\sigma_2(0)$ lies well below the value predicted for a BCS superconductor in the London limit, particularly if the effects of strong coupling are included, which is similar to the observations of others [20]. (In fact, we obtain a term in T^2 in $\lambda(T)$ at low T in all of the YBCO films studied, quite unlike the behavior of conventional superconductors.) If intrinsic, this effect could have important consequences regarding the nature of the pairing state in YBCO. Our results for R_s are somewhat more variable from sample to sample, implying that the low temperature residual losses are still extrinsic. However, R_s continually decreases at the lowest temperatures, rather than

reaching a plateau. It has been shown that oxygen treatment after film growth is an important factor in determining the low temperature R_s of thin films [19], and consequently we expect R_s for our films to decrease further at low T on optimizing our oxygen annealing conditions.

To summarize, we have used the coplanar resonator method to characterize thin films of YBCO. We have calculated the current distribution in the resonators and this allows us to determine the absolute values of the film surface impedance to reasonable accuracy, without relying on fitting to existing theories to fix the value of $\lambda(0)$. Our optimized films appear to be unaffected by patterning damage and have values of R_s comparable to the lowest values reported in the literature for unpatterned films.

REFERENCES

[1] A. Porch, M. J. Lancaster, R. G. Humphreys, and N. G. Chew, "Surface impedance measurements of $YBa_2Cu_3O_7$ thin films using coplanar resonators," *IEEE Trans. Appl. Supercond.*, vol. 3, pp. 1719–1722, 1993.

[2] A. Porch, M. J. Lancaster, R. G. Humphreys and N. G. Chew, "Non-linear microwave surface impedance of patterned $YBa_2Cu_3O_7$ thin films," *J. Alloys and Compounds*, vol. 195, pp. 563–566, 1993.

[3] A. A. Valenzuela and P. Russer, "High Q coplanar transmission line resonator of $YBa_2Cu_3O_{7-x}$ on MgO," *Appl. Phys. Lett.*, vol. 55, pp. 1029–1031, 1989.

[4] G. Gieres, J. Kessler, J. Kraus, B. Roas, P. Russer, G. Solkner, and A. A. Valenzuela, "High-frequency characterisation of $YBa_2Cu_3O_{7-x}$ thin films with coplanar resonators," in *Proc. ISEC '91*, Glasgow, UK, June 1991, pp. 288–291.

[5] W. Rauch, H. Behner, G. Gieres, G. Solkner, F. Fox, A. A. Valenzuela, and E. Gornik, "DC-magnetron sputtering of $YBa_2Cu_3O_{7-\delta}$ thin films for microwave applications," *Physica C*, vol. 198, pp. 389–396, 1992.

[6] W. Rauch, E. Gornik, G. Solkner, A. A. Valenzuela, F. Fox, and H. Behner, "Microwave properties of $YBa_2Cu_3O_{7-x}$ thin films studied with coplanar transmission line resonators," *J. Appl. Phys.*, vol. 73, pp. 1866–1872, 1993.

[7] H. Asano, M. Satoh, and T. Konaka, "High-T_c superconducting $EuBa_2Cu_3O_y$ thin films on MgO and $YAlO_3$ for coplanar devices," *IEEE Trans. Appl. Supercond.*, vol. 3, pp. 1290–1293, 1993.

[8] K. Araki, H. Saito, N. Yuasa, T. Rei, H. Itozaki, and H. Higaki, "Measurement method of high-T_c superconducting planar transmission lines," *IEEE Trans. Magnetics*, vol. 28, pp. 1805–1809, 1992.

[9] C. S. Krafft and C. F. Beckner. "Microwave absorption measurements of high temperature superconductors using a coplanar waveguide," *J. Appl. Phys.*, vol. 69, pp. 4907–4909, 1991.

[10] M. C. Nuss, P. M. Mankiewich. R. E. Howard, B. L. Straughn, T. E. Harvey, C. D. Brandle, G. W. Berkstresser, K. W. Goossen, and P. R. Smith, "Propagation of terahertz bandwidth electrical pulses on $YBa_2Cu_3O_{7-\delta}$ transmission lines on lanthanum aluminate," *Appl. Phys. Lett.*, vol. 54, pp. 2265–2267, 1989.

[11] M. C. Nuss, K. W. Goossen, P. M. Mankiewich, M. L. O'Malley, J. L. Marshall, and R. E. Howard, "Time-domain measurement of the surface resistance of $YBa_2Cu_3O_7$ superconducting films up to 500 GHz," *IEEE Trans. Magetics*, vol. 27, pp. 863–866, 1991.

[12] O. R. Baiocchi, K.-S. Ong, and T. Itoh, "Pulse propagation in super-conducting coplanar striplines," *IEEE Trans. Microwave Theory Tech.*, vol. 40, pp. 509–514, 1992.

[13] G. J. Hofer and H. A. Kratz, "High temperature superconductor coplanar delay lines," *IEEE Trans. Appl. Supercond.*, vol. 3, pp. 2800–2803, 1993.

[14] W. Chew, L. J. Bajuk, T. W. Cooley, M. C. Foote, B. D. Hunt, D. L. Rascoe, and A. L. Riley, "High-T_c superconductor coplanar waveguide filter," *IEEE Electron Device Lett.*, vol. 12, pp. 197–199, 1991.

[15] N. G. Chew, S. W. Goodyear, J. A. Edwards, J. S. Satchell, S. E. Blenkinsop, and R. G. Humphreys, "Effect of small changes in

composition on the electrical and structural properties of $YBa_2Cu_3O_7$ thin films," *Appl. Phys. Lett.*, vol. 57, pp. 2016–2018, 1990.
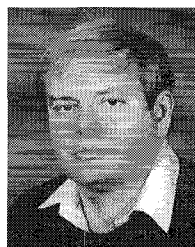
[16] W. T. Weeks, L. L. Wu, M. F. McAllister, and A. Singh, "Resistive and inductive skin effect in rectangular conductors," *IBM J. Res. Dev.*, vol. 23, pp. 652–660, 1979.

[17] D. M. Sheen, S. M. Ali, D. E. Oates, R. S. Withers, and J. A. Kong, "Current distribution, resistance, and inductance for superconducting strip transmission lines," *IEEE Trans. Appl. Supercond.*, vol. 1, pp. 108–115, 1991.

[18] D. E. Oates, A. C. Anderson, D. M. Sheen, and S. M. Ali, "Stripline resonator measurements of Z_s versus H_{rf} in $YBa_2Cu_3O_{7-x}$ thin films," *IEEE Trans. Microwave Theory Tech.*, vol. 39, pp. 1522–1529, 1991.

[19] N. Klein, U. Poppe, N. Tellmann, H. Schulz, W. Evers, U. Dahne, and K. Urban, "Microwave surface impedance of epitaxial $YBa_2Cu_3O_7$ films below $T_c/2$," *IEEE Trans. Appl. Supercond.*, vol. 3, pp. 1102–1109, 1993.

[20] Z. X. Ma, R. C. Taber, L. W. Lombardo, A. Kapitulnik, M. R. Beasley, P. Merchant, C. B. Eom, S. Y. Hou, and J. M. Phillips, "Microwave penetration depth measurements on $Bi_2Sr_2CaCu_3O_8$ single crystals and $YBa_2Cu_3O_{7-\delta}$ thin films," *Phys. Rev. Lett.*, vol. 71, pp. 781–784, 1993.

Michael J. Lancaster (M'91) was educated at Bath University, UK, where he graduated in physics in 1980. His postgraduate research continued at Bath, where he was awarded his Ph.D. in 1984 for research into non-linear underwater acoustics.

He joined the surface acoustic wave research group at the Department of Engineering Science at Oxford University as a research fellow in 1984. In 1987 he joined the School of Electronic and Electrical Engineering at Birmingham University, UK, as a lecturer in electromagnetic theory. Shortly after this he began his research into the physics, characterization and application on HTS materials at microwave frequencies. Currently he heads the HTS microwave group in the School, and his present interests include HTS antennas, miscellaneous microwave filters, and the measurement of the microwave properties of superconductors.

Adrian Porch was educated at Cambridge University, where he graduated in physics in 1986. His postgraduate research was performed in the Low Temperature Physics Group at the Cavendish Laboratory, Cambridge University, and he was awarded his Ph.D. in 1991 for his research into the high frequency properties of high temperature superconductors (HTS).

Since 1990 he has been a research fellow at Birmingham University, UK, working in the interdisciplinary superconductivty research group, specifically studying the fundamental properties and applications of HTS materials at microwave frequencies.

Dr. Porch is a member of the UK Institute of Physics.

Richard G. Humphreys graduated from Cambridge University in 1971, and was awarded a Ph.D. from Bath University, UK, in 1975.

He then worked at the Max Plank Institute für Festkorperforschung in Stuttgart for two years, followed by some months at the high magnetic field laboratory in Grenoble. Since then he has worked at DRA, Malvern, UK. His interests have progressed from the properties of semiconductors to devices made from them, particularly infrared detectors, and since 1987 to HTS devices.